Coulomb Dissociation and Momentum Distributions for ^{11}Li → ^{9}Li+n+n Breakup Reactions

ANL/PHY/CP--78842

DE93 008651

Henning Esbensen

Physics Division, Argonne National Laboratory, Argonne, IL 60439,U.S.A.

Abstract. Momentum distributions for the ^{11}Li → ^{9}Li+n+n breakup reaction, generated by Coulomb dipole excitations, are calculated in a 3-body model for ^{11}Li. The relative momentum distribution of the two neutrons is in good agreement with recent 3-body coincidence measurements but the momentum distribution for the ^{9}Li recoil and the decay energy spectrum are much narrower than observed. These discrepancies may be due to higher order dynamical effects which have been ignored.

1. Introduction

The construction of the secondary beam facilities at RIKEN, GANIL, Michigan State University and at GSI has made it possible to study the properties of nuclei far from stability. A large effort has been devoted to the study of light, neutron rich nuclei, and the aim has been to extract information about the structure properties of these nuclei from measurements of fragmentation reactions.

A particularly interesting example is the nucleus ^{11}Li. It has only one bound state and it contains two loosely bound valence neutrons. Correlations between the valence neutrons must play a prominent role for the binding of this nucleus since ^{10}Li is unbound. One of the best ways to probe the structure of ^{11}Li, associated with the loosely bound valence neutrons, is to study (^{11}Li,^{9}Li) breakup reactions. The cross section is very large for a heavy target like lead (several barns at intermediate energies), and it is dominated by Coulomb excitations of the low-lying dipole response. This is very fortunate since Coulomb excitation is a well understood reaction mechanism, which provides a close connection between reaction data and the dipole response of ^{11}Li.

Many different measurements of (^{11}Li,^{9}Li) reactions have been performed in recent years. They include measurements of cross sections for various targets [1], momentum distributions of the ^{9}Li fragment [2,3], and of the single-neutrons emitted in the reaction [4,5], and finally also the first complete 3-body coincidence measurements of the ^{9}Li fragment and two neutrons [6,7,8].

The simplest theoretical approach, which focuses directly on a realistic description of the valence neutrons and which may be applied to describe the available (^{11}Li,^{9}Li) reaction data, is to describe ^{11}Li as a 3-body system, consisting of an inert ^{9}Li core and

DISCLAIMER

two interacting neutrons. This approach requires as input a realistic n-n and n-core interaction. The n-n interaction is well known from low-energy n-n scattering, but there has been some uncertainty in the n-core interaction because of a poor knowledge of the structure of the unbound nucleus ^{10}Li. There are at least two groups that have taken this approach, based on Faddeev calculations [9,10] and on the two-particle Green's function method [11,12], respectively.

In my talk I will discuss the results obtained from the 3-body model that is based on the two-particle Green's function method. I will make comparisons to the predictions obtained from Faddeev calculations and to the available data, in particular to those obtained in the 3-body coincidence measurements reported in Ref. [8].

2. Two-particle Green's function method

The two-particle Green's function technique has been applied to study the ground state [11] and the dipole response [12] of ^{11}Li and similar nuclei that consist of an inert core and two interacting valence neutrons. I shall here summarize the main ingredients of the model. The starting point is a two-particle Hamiltonian of the form

$$H_2(\mathbf{r}_1,\mathbf{r}_2) = H_1(\mathbf{r}_1) + H_1(\mathbf{r}_2) + v(\mathbf{r}_1,\mathbf{r}_2), \tag{1}$$

where H_1 is the single-particle Hamiltonian for a valence neutron interacting with the core, and $v(\mathbf{r}_1,\mathbf{r}_2)$ is the interaction between the two valence neutrons. The single-particle Hamiltonian is parameterized in the usual way, with a kinetic energy operator, Wood-Saxon potential and spin-orbit interaction. It is adjusted to describe known properties (bound states or scattering states) of the n-core system. In the case of ^{11}Li, it has been adjusted to produce a $p_{1/2}$ resonance in ^{10}Li at 0.8 MeV. It is noted that it is very difficult in the present approach to treat the full effect of the core motion exactly and it has therefore been neglected in the Hamiltonian (1).

The n-n interaction is parameterized as a density-dependent contact interaction,

$$v(\mathbf{r}_1,\mathbf{r}_2) = \delta(\mathbf{r}_1-\mathbf{r}_2)(v_0 + v_\rho(\frac{\rho_c(\mathbf{r}_1)}{\rho_0})^P), \tag{2}$$

where ρ_c is the nuclear density of the core and $\rho_0 = 0.16$ fm^{-3}. A contact interaction is only meaningful in a truncated space of two-particle states, and we have chosen a cutoff at $E_c = 40$ MeV. The strength of the density-independent part of the interaction, v_0, has been chosen to give an infinite scattering length. This is slightly stronger than the empirical n-n interaction, which gives a scattering length of about -17 fm. The parameters for the density-dependent part of the interaction, v_ρ and P, have been adjusted so that the calculations described in the following reproduce the binding of ^{12}Be and ^{14}C. We find that the resulting effective n-n interaction essentially vanishes inside the core.

The use of a contact interaction simplifies the calculation of the ground state and excited states considerably. For a total angular momentum (JM) of the two valence neutrons one can construct the non-interacting two-particle Green's function

$$G^{(0)}_{JM}(E) = (H_1(1) + H_1(2) - E - i\eta)^{-1} = \sum \frac{|(j_1 j_2)_{JM}\rangle\langle(j_1 j_2)_{JM}|}{e_1 + e_2 - E - i\eta}. \tag{3}$$

The sum is over all two-particle states $(e_1\ell_1 j_1; e_2\ell_2 j_2)$ which are below the cutoff, $e_1+e_2 \leq E_c$, and excludes states that are occupied by core neutrons. The correlated Green's

function can now be constructed from

$$G_{JM}(E) = (H_1(1) + H_1(2) + v - E - i\eta)^{-1} = (1 + G^{(0)}_{JM}(E)v)^{-1} G^{(0)}_{JM}(E). \qquad (4)$$

This Green's function describes the dynamical propagation of two neutrons with the total energy E, interacting with each other and with the core. It is a function of four coordinate positions, $(\mathbf{r}_1, \mathbf{r}_2)$ and $(\mathbf{r}'_1, \mathbf{r}'_2)$, but since we use a contact interaction it is actually sufficient to construct the inverse of the operator $(1 + G^{(0)}_{JM}(E)v)$ for $r_1 = r_2$ and $r'_1 = r'_2$. Thus the calculations become quite similar to those performed in ordinary RPA calculations for particle-hole excitations [13] and the inverse operator can be constructed in a two-dimensional, radial coordinate space.

Ground state of ^{11}Li

The ground state of the two valence neutrons is a 0^+ state (we ignore the spin of the core), and the ground state energy is the lowest pole of the associated correlated Green's function. The ground state wave function, $|\Psi_{gs}\rangle$, can also be extracted from this Green's function (see Ref. [11] for details). Adjusting the n-core interaction to produce a $p_{1/2}$ resonance at 0.8 MeV, as suggested by the measurement of Wilcox et al. [14], the model predicts a two-neutron separation energy of 0.20 MeV for ^{11}Li, a RMS distance of 6.24 fm between the two valence neutrons, and a RMS distance of 4.93 fm between their center of mass and the ^{9}Li core.

It is interesting to compare these results to the predictions obtained from Faddeev calculations [9,10] which treat the 3-body kinematics correctly. The calculations are based on a somewhat stronger n-core interaction, with a $p_{1/2}$ resonance close to 0.5 MeV, and a more realistic, finite range n-n interaction. The resulting two-neutron separation energy is 0.21 MeV, and the RMS distance between the two valence neutrons is 6.32 fm, in good agreement with our results. The RMS distance between the core and the center of mass of the two valence neutrons is 4.48 fm, which is smaller than our result as one would expect for a stronger n-core interaction.

Recent measurements [15,16] indicate that the neutron resonance in ^{10}Li is close to 0.65 MeV. This is lower than the earlier measurement [14], which we used to calibrate our n-core interaction. A recent measurement [17] also indicates that the two-neutron separation energy for ^{11}Li is somewhat larger ($S_{2n} = 0.34 \pm 0.05$ MeV) than the value we predict. The new measurement is consistent with the result obtained by Wouters et al. [18] ($S_{2n} = 0.33 \pm 0.12$ MeV), but it is significantly larger than the old result, of 0.17 ± 0.08 MeV, measured by Thibault et al. [19].

It is obvious that if we adopt a lower $p_{1/2}$ resonance in our calibration of the n-core interaction we would also obtain a larger binding energy. We have chosen not to change the calibration of our model at present, since we find it important to have a consistent set of results, which are based on identical assumptions. In future calculations, it would be useful to modify not only the n-core interaction but also the the n-n interaction. The density independent part is too strong, since it produces an infinite scattering length. It would also be better to use for example ^{6}He to calibrate the density dependent part of the interaction, instead of ^{12}Be and ^{14}C, since deformation of the core may play a significant role for these two nuclei.

Dipole Response

Having determined the ground state wave function, Ψ_{gs}, we can now calculate the dipole response of the valence neutrons. The effective dipole operator is

$$D_\mu = -\frac{Ze}{A}(r_1 Y_{1\mu}(\hat{r}_1) + r_2 Y_{1\mu}(\hat{r}_2)), \tag{5}$$

and the dipole matrix element to a specific two-particle final state is

$$M^{(0)}(E1,\mu) = \langle (j_1 j_2)^1_\mu | D_\mu | \Psi_{gs} \rangle, \tag{6}$$

where the two single-particle final states are solutions to the n-core Hamiltonian. We have here ignored the interaction between the two neutrons in their final state. It is actually possible, within our model, to include this interaction to all orders. To do this we first note that the free propagation of the two neutrons, after they have been excited by the dipole field, is governed by the non-interacting Green's for J=1, given in Eq. (3) and evaluated at the two-particle energy, $E = e_1 + e_2$. The effect of the final state n-n interaction can now be treated in terms of a series of successive propagation and scattering of the two neutrons. The resulting "correlated" dipole matrix element is,

$$\begin{aligned} M(E1,\mu) &= \langle (j_1 j_2)^1_\mu | \Big(1 - vG^{(0)}_{1\mu}(E) + vG^{(0)}_{1\mu}(E) vG^{(0)}_{1\mu}(E) - ...\Big) D_\mu | \Psi_{gs} \rangle \\ &= \langle (j_1 j_2)^1_\mu | \Big(1 + vG^{(0)}_{1\mu}(E)\Big)^{-1} D_\mu | \Psi_{gs} \rangle, \end{aligned} \tag{7}$$

where we have expressed the scattering series in a closed form. Summing over all final states (f.st.) one can now derive the following compact expression for the dipole response,

$$\begin{aligned} \frac{dB(E1)}{dE} &= \sum_{\mu, f.st.} |M(E1,\mu)|^2 \delta(E - e_1 - e_2) \\ &= \frac{1}{\pi}\, Im \sum_\mu \langle \Psi_{gs} | D^*_\mu G_{1\mu}(E) D_\mu | \Psi_{gs} \rangle, \end{aligned} \tag{8}$$

which contains the correlated Green's function defined in Eq. (4). A detailed derivation, and also a discussion of the numerical technique used to calculate this response, is given in Ref. [12].

The total strength we obtain is 1.57 e^2 fm^2. This is slightly smaller than the sum rule value,

$$B(E1) = \frac{3}{4\pi}\left(\frac{Ze}{A}\right)^2 \langle r_1^2 + r_2^2 + 2\mathbf{r}_1 \cdot \mathbf{r}_2 \rangle, \tag{9}$$

which is related to the mean square distance between the core and the center of mass of the two neutrons in the ground state. The sum rule strength is 1.73 e^2 fm^2. It includes contributions from the forbidden transitions to occupied core states, which are excluded explicitly in the actual response. The total strength obtained from Faddeev calculations [10] ranges from 1 to 1.4 e^2 fm^2, which is slightly smaller than our prediction in accord with the smaller RMS radius.

The dipole response of ^{11}Li is shown by the fully drawn curve in Fig. 1 (left panel). The dotted-dashed curve shows the response we obtain when we ignore the effect of the n-n interaction in excited states. Clearly, the final state interaction has a very dramatic effect on the response and shifts the strength to lower excitations. However,

the total strengths of the two distributions are identical. The dashed curve in Fig. 1 shows the dipole response obtained from an independent particle model which has been adjusted to reproduce the ground state single-particle density we obtain from the two-particle Green's function method. The shape of this response is similar to the correlated response at low excitations but the total strength of the correlated response is about 50% larger. This enhancement can easily be explained by the sum rule (9). The RMS radii of the valence neutrons are identical in the two models (by construction) but the last term in (9), $2\langle \mathbf{r}_1 \cdot \mathbf{r}_2 \rangle$, which vanishes in the independent particle model, gives an additional 50% contribution to the total strength of the correlated response. It is also interesting to note that the last term in Eq. (9) would be identical to the first two terms if we assume that the two neutrons form a point particle.

One can also extract the dipole strength as a differential in the kinetic energies (in the rest frame of ^{11}Li) of the two emitted neutrons [12]. This quantity is illustrated in Fig. 1 (right panel) as a contour plot. The maximum of the strength function is not shown in the figure; it is located at $e_1 = e_2 = 80$ keV. An interesting feature of this plot is the ridges that appear around 0.7 MeV. They disappear when the final states are replaced by plane waves (see Fig. 3 in Ref. [12]). The ridges reflect the physical process in which one of the neutrons is emitted with a large kinetic energy whereas the other neutron remains as a spectator near the $p_{1/2}$ resonance of ^{10}Li. It would be very useful to get information about the structure of the unbound nucleus ^{10}Li from measurements of this kind, i. e. from coincidence measurements of the 3-body breakup reaction (^{11}Li,^{9}Li+n+n) induced by the Coulomb field from a high Z target. This reaction mechanism is simpler and better understood (as we shall see in the next section) than the multi-nucleon exchange reactions that have been used up till now [14-16].

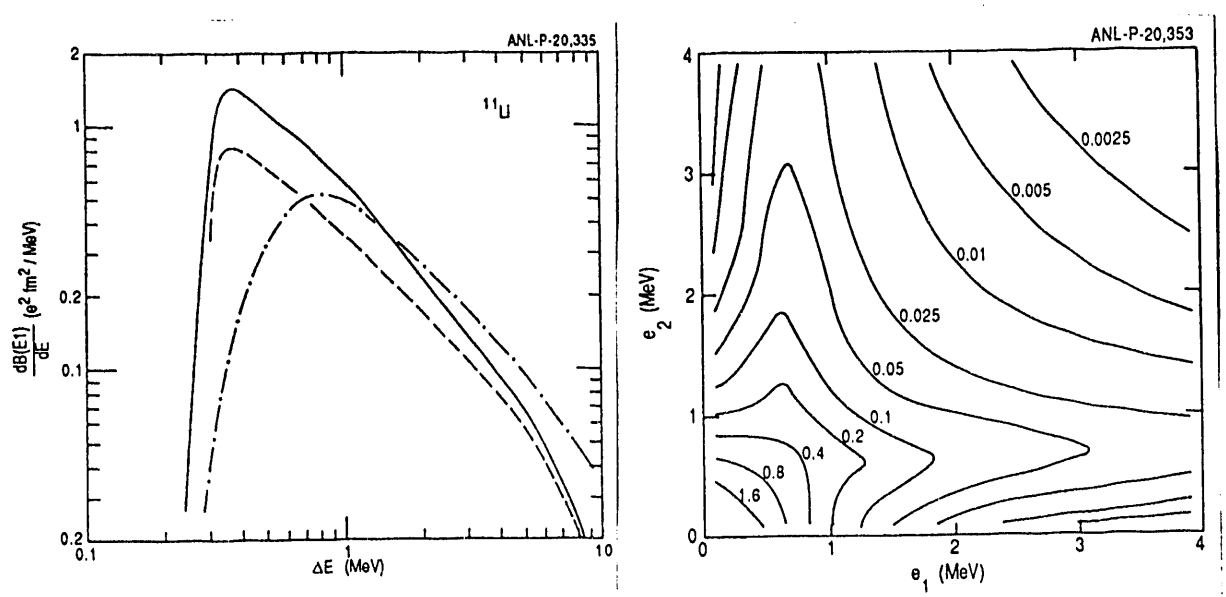

Fig. 1. Calculated dipole strength of the valence neutrons in ^{11}Li. The left panel shows the correlated response (fully drawn curve), the response obtained by ignoring the n-n interaction in the final state (dot-dashed curve), and the independent-particle response (dashed curve), as functions of excitation energy. The right panel is a contour plot of the correlated response as a function of the energies of the two emitted neutrons.

3. Coulomb Dissociation and Momentum Distributions

We have previously calculated the cross section for (^{11}Li,^{9}Li) reactions on different targets at 800 MeV/u [20], and found a surprisingly good agreement with the data [1]. Almost 60% of the calculated cross section for a lead target is due to Coulomb dissociation, generated by excitations of the dipole response illustrated in Fig. 1. At lower energies we expect that an even larger fraction of the cross section is due to this reaction mechanism. It is therefore reasonable to analyze the 3-body coincidence measurements [8], obtained at 28 MeV/u on a lead target, in terms of Coulomb dissociation. Moreover, the data analysis [8] suggests that the nuclear part of the breakup is strongly suppressed in the measured 3-body events, consisting of a ^{9}Li fragment in coincidence with two neutrons.

We have also studied the angular correlation between the two neutrons emitted in (^{11}Li,^{9}Li) reactions [12] and we have recently applied this formalism to calculate the associated momentum distributions in the rest frame of the excited ^{11}Li nucleus [21]. The basic cross section can be expressed as a differential in the momenta of the two neutrons as follows,

$$\frac{d^6\sigma}{d\mathrm{k}_1 d\mathrm{k}_2} = g_L(\xi)\frac{d^6B^L(E1)}{d\mathrm{k}_1 d\mathrm{k}_2} + g_T(\xi)\frac{d^6B^T(E1)}{d\mathrm{k}_1 d\mathrm{k}_2}. \tag{10}$$

This cross section has two components, a longitudinal (L) and a transverse (T), which are generated by the Coulomb force from the target nucleus, acting along the beam direction and perpendicular to the beam direction, respectively. The magnitudes of the two components are determined by the functions,

$$g_L(\xi) = (\frac{4\pi Z_T e}{3\hbar v})^2\xi^2(K_1^2(\xi) - K_0^2(\xi))(1-(v/c)^2), \tag{11a}$$

$$g_T(\xi) = (\frac{4\pi Z_T e}{3\hbar v})^2\xi^2(K_0^2(\xi) - K_1^2(\xi) + \frac{2}{\xi}K_0(\xi)K_1(\xi)), \tag{11b}$$

where ξ is the adiabaticity parameter, which depends on the excitation energy ΔE, $\xi = R\Delta E/(\hbar\gamma v)$, and R is determined by the minimum impact parameter for which a strong nuclear absorption sets in, c.f. Eq. (5.10) of Ref. [12].

We have introduced two dipole strength distributions in Eq. (10), a longitudinal and a transverse, which depend on the directions of the two momenta. If one integrates the two distributions over all orientations one obtains the same result, which is (trivially) related to the dipole strength distribution illustrated in Fig. 1. The longitudinal distribution is defined by,

$$\frac{d^6B^L(E1)}{d\mathrm{k}_1 d\mathrm{k}_2} = \frac{3}{k_1^2k_2^2}\sum_{h_1h_2}|f^{10}_{h_1h_2}(\mathrm{k}_1,\mathrm{k}_2)|^2, \tag{12}$$

where the sum is over the helicities of the two neutrons. The expression for the f-amplitudes is fairly complicated. It is given in Ref. [12] in terms of dipole matrix elements, phase shifts of the two emitted neutrons and two-particle D-functions. The distribution is invariant under rotations around the beam direction. The symmetry axis for the transverse component is perpendicular to the beam direction and falls in the scattering plane determined by the incident projectile and the target nucleus. The two distributions are otherwise identical, i. e. they are related by a simple rotation

of 90°. We shall make use of this fact in the following. It is important to realize that transverse dipole excitations dominate the (^{11}Li,^{9}Li) Coulomb dissociation cross section at intermediate energies; they generate 78% of the cross section at 28 MeV/u on lead, and 95% at 800 MeV/u.

Let us first consider the spherical part of the momentum distributions associated with the ^{9}Li recoil and with the relative motion of the two neutrons. Using the fact that the transverse dipole strength distribution can be obtained from the longitudinal by a simple rotation of 90°, we can obtain for the following expressions for the two momentum distributions, expressed in terms of the longitudinal dipole strength,

$$\frac{d\sigma}{d|\mathbf{p}_1 \pm \mathbf{p}_2|} = \int d\mathbf{k}_1 d\mathbf{k}_2 \; (g_L(\xi) + g_T(\xi)) \frac{d^6 B^L(E1)}{d\mathbf{k}_1 d\mathbf{k}_2} \delta(|\mathbf{p}_1 \pm \mathbf{p}_2| - |\mathbf{k}_1 \pm \mathbf{k}_2|). \qquad (13)$$

When comparing to the data we also include the detection efficiency. It has been parameterized as a simple function of the decay energy, c. f. Fig. 11 in Ref. [8], and it can therefore easily be included in the calculations. The two distributions we obtain are shown in Fig. 2 together with the data [8]. The calculated distributions have arbitrarily been normalized to 100, and the data points were normalized to minimize the χ^2. The data for the relative motion of the two neutrons are in surprisingly good agreement with our calculation, whereas the measured recoil momentum distribution is shifted to higher momenta and has a significantly larger width.

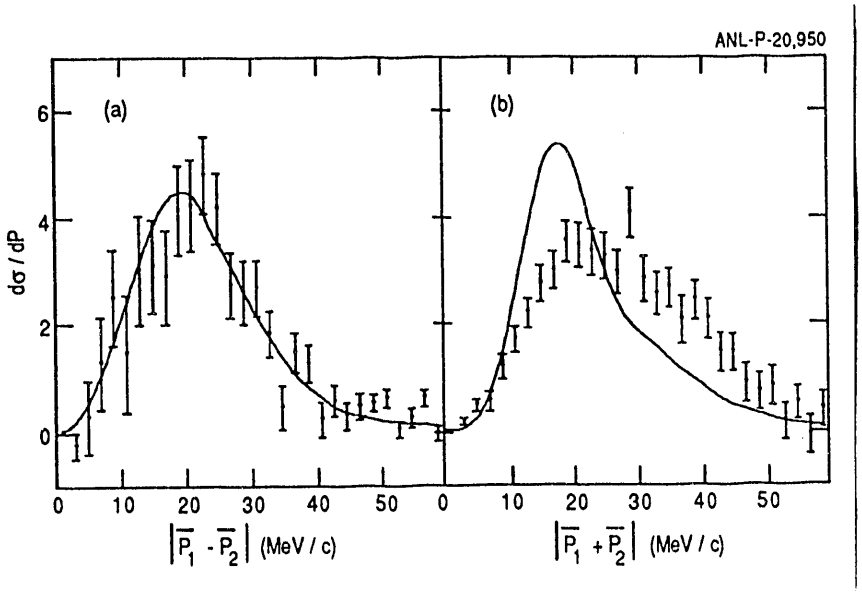

Fig. 2. Momentum distributions for the relative motion of the two neutrons (A) and the ^{9}Li recoil (B) in the rest frame of the ^{11}Li $\rightarrow$ ^{9}Li+n+n breakup reaction on lead at 28 MeV/u. The data are from Ref. [8]. The calculated curves (normalized to 100) include the detection efficiency.

The calculation of the decay energy spectrum is even simpler, since the angle integration over the orientations of the two momenta becomes trivial,

$$\frac{d\sigma}{dE} = \big(g_L(\xi) + g_T(\xi)\big) \frac{dB(E1)}{dE}. \qquad (14)$$

The result (including detection efficiency) is shown in Fig. 3 of Ref. [21] together with the data. The measured spectrum is shifted towards higher excitations when compared to the model prediction. The shift is similar to that observed for the recoil momentum distribution shown in Fig. 2B. In fact, the discrepancies are probably related.

It was noted in Ref. [8] that the average velocity of the ^{9}Li fragments is larger than the average velocity of the two neutrons. This was ascribed to a post acceleration effect on the ^{9}Li fragment, when it is liberated in close vicinity of the target nucleus, and it was interpreted in terms of a life-time, which is much shorter than what one would expect from the width of the low-lying dipole response (see Ref. [8] for details). Our calculations, which are based on first order perturbation theory, do not include a post acceleration effect. The measured momentum distribution shown in Fig. 2B has been corrected for the average velocity shift. The post acceleration effect will also lead to fluctuations in the velocity of the heavy fragment but it is not possible to correct for that. There may also be additional fluctuations for example from energy loss in the target. The discrepancy between our predictions and the data may be due to these fluctuations. In this connection, it is important to emphasize that the data for the relative motion of the two neutrons are insensitive to post acceleration effects, and they are in good agreement with our prediction, c. f. Fig. 2A.

Let us also make a comparison to the total cross sections measured in Ref. [8]. The Coulomb dissociation cross section we obtain is $\sigma_C = 4.5$ b. We expect that the nuclear part of the (^{11}Li,^{9}Li) cross section is of the order of $\sigma_{nuc} = 1\pm0.3$ b, based on the independent-particle model calculations performed by Sustich [22]. He also assumed a two-neutron separation energy of 0.2 MeV but spatial correlations between the two valence neutrons may reduce his estimate slightly, c. f. Ref. [20]. Our estimated total cross section is 5.5 b, which is slightly higher than the 5.1 ± 0.3 b obtained from the telescope data. The neutron coincidence measurements appear to be insensitive to large decay energies, say larger than 1.5 MeV. The Coulomb dissociation cross section we obtain with this cut-off is $\hat{\sigma}_C = 3.9$ b, which can be compared to the 3.6 ± 0.4 b obtained from the two-neutron coincidence data. This does not leave much room for nuclear induced reactions. The measured single-neutron cross section is 8.3 ± 0.5 b. This can be compared to our estimate of $2\hat{\sigma}_C + \sigma_{nuc} = 8.8$ b, assuming for simplicity that the neutron multiplicities for Coulomb and nuclear induced reactions are 2 and 1, respectively. The three estimated cross sections are in reasonable agreement with the measured values but they are all slightly larger. This trend may be related to the fact that the experimental binding energy [17] is somewhat larger than our model prediction.

An interesting question is whether the angular correlation between the two neutrons has any effect on the distributions with respect to the two momenta, $|\mathbf{p}_1 \pm \mathbf{p}_2|$. The total spread of these two momenta are essentially identical in the experiment [8] and our model predicts the same result (within 6-8 %, the spread of $\mathbf{p}_1 - \mathbf{p}_2$ being the larger). This result does not necessarily mean that the momenta of the two neutrons are uncorrelated. A possible way to see an effect of angular correlations is to study the different components of the momentum distribution for the ^{9}Li recoil. We have discussed that in Ref. [21] and the following is a summary of the results we obtained. Thus, one can decompose the recoil momentum distribution into three orthogonal components, a longitudinal (along the beam direction) and two transverse,

$$\frac{d\sigma}{dP_i} = \int d\mathbf{k}_1 d\mathbf{k}_2 \frac{d^6\sigma}{d\mathbf{k}_1 d\mathbf{k}_2} \delta(P_i + k_{1,i} + k_{2,i}), \quad i = 1,2,3. \tag{15}$$

The longitudinal component (i=3) has been measured by Orr et al. [3], and our model

(including the effect of angular correlations) reproduce the data very well. The two transverse components are an out-of-plane (i=1) and an in-plane (i=2) distribution, where the plane in question is the scattering plane defined by the incident projectile and the target nucleus.

The longitudinal and transverse in-plane distributions are illustrated in Fig. 4 for 28 MeV/u on a lead target. The longitudinal distribution (fully drawn curve) has a maximum at zero, whereas the transverse in-plane distribution (dashed curve) has a local minimum at zero. These features can be understood from the angular correlations discussed in Ref. [12]. There it was found that the emission probability is enhanced when the two neutrons are emitted on opposite sides of the symmetry axis, with an opening angle close to 90°. For this configuration one finds that the component of the ^{9}Li recoil momentum, which is along the symmetry axis, is generally larger than the other two perpendicular components. This trend is consistent with the results shown in Fig. 3, since the relevant symmetry axis is the in-plane transverse direction because of the dominance of transverse dipole excitations. The transverse out-of-plane distribution is not shown. It is similar to the longitudinal momentum distribution and peaks at zero. A detailed discussion of these results is given in Ref. [21].

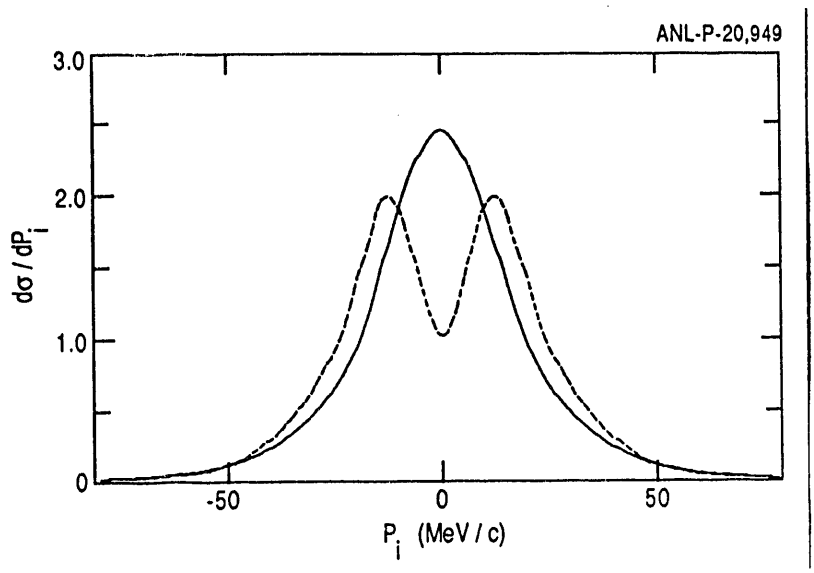

Fig. 3. Calculated longitudinal (fully drawn curve) and transverse in-plane (dashed curve) momentum distributions for the ^{9}Li recoil in (^{11}Li,^{9}Li) reactions on lead at 28 MeV/u. The distributions have been normalized to 100.

Finally, it is also interesting to study the energy dependence of the longitudinal momentum distribution for the ^{9}Li recoil. The naive expectation is that the width of this distribution will increase with increasing beam energy, simply because the average excitation energy increases. This is indeed the case if we ignore the angular correlation between the emitted neutrons. However, if we include this correlation, as we did in Fig. 3, the width decreases slightly [21], from 34 to 32 MeV/c (FWHM) going from 28 to 800 MeV/u. It will be interesting to see whether experiments will confirm this trend.

4. Conclusions

The ^{11}Li→^{9}Li+n+n breakup reaction on a heavy target is dominated by Coulomb dipole excitations at intermediate energies. This reaction mechanism, combined with a previously developed 3-body model for ^{11}Li, provides a good description of the momentum distribution for the relative motion of the two emitted neutrons obtained in recent 3-body coincidence measurements. The calculated momentum distribution for the ^{9}Li recoil and the decay energy spectrum are much narrower than measured. These discrepancies may be related to Coulomb acceleration effects, which can only be treated in a higher order reaction theory. Calculations indicate that the different components of the ^{9}Li recoil momentum distribution may contain important information about the angular correlation between the two emitted neutrons.

Acknowledgment. The author is grateful for the hospitality of the staff at the National Superconducting Cyclotron Laboratory at Michigan State University. The author is also grateful to A. Galonsky, K. Ieki and D. Sackett for discussions and to George Bertsch for his continued collaboration. This work was supported by the U.S. Department of Energy, Nuclear Physics Division under Contract No. W-31-109-ENG-38.

References

[1] Kobayashi T et al., *Phys. Lett. B* **232**, 51 (1989).
[2] Kobayashi T et al., *Phys. Rev. Lett.* **60**, 2599 (1988).
[3] Orr N A et al., *Phys. Rev. Lett.* **69**, 2050 (1992).
[4] Anne R et al., *Phys. Lett. B* **250** 19, (1990); *Nucl. Phys. A* **540** 365, (1992).
[5] Kobayashi T, to be published.
[6] Shimoura S et al., to be published.
[7] Ieki K, Sackett D, Galonsky A et al., submitted for publication.
[8] Sackett D, Ieki K, Galonsky A et al., submitted for publication.
[9] Bang J M and Thompson I J, *Phys. Lett B* **279**, 201 (1992).
[10] Bang J M, Ferreira L S and Maglione E, *Europhys. Lett.* **18**, 679 (1992).
[11] Bertsch G F and Esbensen H, *Ann. Phys.* **209**, 327 (1990).
[12] Esbensen H and G F Bertsch, *Nucl. Phys. A* **542**, 310 (1992).
[13] Bertsch G and Tsai S F, *Physics Reports C* **18**, 125 (1975).
[14] Wilcox K H et al., *Phys. Lett. B* **59**, 142 (1975).
[15] Bohlen H G et al., to be published.
[16] Benenson W, private communications.
[17] Kobayashi T, *Nucl. Phys. A* **538**, 343c (1992).
[18] Wouters et al., *Z. Phys. A* **331**, 229 (1988).
[19] Thibault et al., *Phys. Rev. C* **12**, 644 (1975).
[20] Esbensen H and Bertsch G F, *Phys. Rev C* **46**, 1552 (1992).
[21] Esbensen H, Bertsch G F, and Ieki K, submitted for publication.
[22] Sustich A, *Z. Phys. A* **342**, 31 (1992).

END

DATE
FILMED
5/11/93